RSC Advances

ROYAL SOCIETY OF CHEMISTRY

www.rsc.org/advances

Effect of hematite addition to $CaSO_4$ oxygen carrier in chemical looping combustion of coal char

Ning Ding[a,b*], Chengwu Zhang[a], Cong Luo[b], Ying Zheng[b*], Zhigang Liu[a]

[a]Energy Research Institute of Shandong Academy of Sciences, Jinan, 250014, China

[b]State Key Laboratory of Coal Combustion, School of Energy and Power Engineering, Huazhong University of Science and Technology, Wuhan, 430074, China

Abstract: Chemical looping combustion (CLC) is a very promising technology combined with the potential of reducing the costs and energy penalty dramatically for CO_2 capture. For $CaSO_4$ oxygen carrier, the low reactivity and the sulfur species evolution limit its practical application in CLC. In this paper, $CaSO_4$ oxygen carriers decorated with hematite were prepared by mechanical blending method with natural anhydrite as active support and hematite as additive. Experiments of gasification and CLC of coal char in steam medium were conducted in a laboratory scale fluidized-bed reactor at atmospheric pressure. The effects of reaction temperature, iron-sulfur ratio and cycle numbers on the performance of $CaSO_4/Fe_2O_3$ oxygen carriers were investigated in terms of the carbon conversion, the CO_2 yield as well as the SO_2 evolution rate. Temperature and hematite favored an enhancement of the carbon conversion and CO_2 yield. The SO_2 evolution increased with the rising reaction temperature, but the peak time was delayed which was ascribed to the suppressed sulfur effect of hematite. The iron-sulfur ratio had little influence on the product gas concentrations, and there was no obvious decrease for the SO_2 evolution rate when the iron-sulfur ratio reached 0.13. Redox cyclic tests showed the cumulative evolution rates of SO_2 in the reduction/oxidization decreased firstly and increased subsequently with the increase of cycle number. The related chemical equations involving the oxygen-transfer mechanism of iron-catalyzed reduction were proposed.

* Corresponding author. Tel: +86-531-85599030. Fax: +86-531-82961954.
E-mail address: 864911600@163.com (N. Ding). Y.Zheng1967@gmail.com (Y. Zheng)

Keywords: CO_2 Capture; Chemical Looping Combustion; $CaSO_4/Fe_2O_3$ Oxygen Carrier; Sulfur Evolution

1. Introduction

It is well known that fossil fuel consumption is the major source of anthropogenic CO_2 emission. There are a number of techniques that can be used to separate CO_2 from the burning, but most need the large amount of energy for the separation and compression [1-3]. Chemical looping combustion (CLC) is a new combustion technology where CO_2 is separated from the flue gases without such an energy consuming gas separation process [4-6].

CLC involves the use of oxygen carrier which transfers oxygen from air to the fuel, and typically employs a dual fluidized bed system: an air reactor (AR) and a fuel reactor (FR) [7]. In the FR, the fuel (natural gas, refinery gas, synthesis gas from coal gasification, etc.) is oxidized by an oxygen carrier, thus producing an outlet gas of concentrated CO_2 and steam. After condensation, almost pure CO_2 can be obtained without any loss of energy during the separation. The reduced oxygen carrier is transferred to the AR where it is oxidized, while emitting a large amount of heat and producing high temperature gases consisting of N_2 and residual O_2. The oxygen carrier regenerated is recirculated to the FR for a new cycle, thereby avoiding direct contact between fuel and air. The reduction is either endothermic or slightly exothermic depending on the type of oxygen carrier and fuel. The total amount of heat evolved from the two reactions is equivalent to that of normal combustion of the same fuel [8-10].

At present, many researchers pay more attention to the utilization of solid fuels (such as coal and biomass) into CLC process [11, 12] because solid fuels are more abundant and less expensive than gaseous fuels. There are two routes to realize CLC by solid fuels. Solid fuels can be used in CLC if they are first gasified by a separate gasification process and then oxidized in the FR. The disadvantages of the first route are the difficulties associated with gasification and the need for an

energy intensive air separation unit. The second route is to introduce directly solid fuels to the FR [8]. Solid fuels should be gasified firstly by steam or CO_2 to produce syngas, and oxygen carrier subsequently reacts with syngas to produce CO_2 and H_2O. Despite its many technical obstacles, the second route is becoming more and more accepted [13-16].

The oxygen carrier should satisfy several requirements: low cost, high oxygen transfer capacity and selectivity toward CO_2 and H_2O, high reactivity during the cyclic test, high mechanical strength, high resistance to agglomeration and sintering, and environmental friendly [17]. Recently a $CaSO_4$ oxygen carrier has attracted increasing attention as a potential oxygen carrier for CLC, because of its high oxygen transport capacity and low cost. ALSTOM Power Co. Ltd. [18] developed the limestone based chemical looping process, and the plant facility at a scale of 3 MW_{th} fuel power using $CaSO_4$ as an oxygen carrier is in debugging and operating stage. Tian and Guo [19] investigated the influence of the partial pressure of CO on the reduction behavior. Wang and Anthony [20] proposed solid fuels gasification combined with CLC of $CaSO_4$ oxygen carrier for the clean combustion. A research group led by Shen and Xiao at the Southeast University in China also investigated the feasibility of $CaSO_4$ as an oxygen carrier [21], reactivity test with gaseous and solid fuels [22, 23], and the reduction kinetics [24, 25]. The thermodynamic and experimental results demonstrated $CaSO_4$ oxygen carrier may be an alternative oxygen carrier with high oxygen capacity. The main reactions take place in the FR (R1-R3) and the AR (R4) which are listed as follows:

$$CaSO_4 + 4H_2 \rightarrow CaS + 4H_2O \quad \text{(R1)}$$

$$CaSO_4 + 4CO \rightarrow CaS + 4CO_2 \quad \text{(R2)}$$

$$CaSO_4 + CH_4 \rightarrow CaS + CO_2 + 2H_2O \quad \text{(R3)}$$

$$CaS + 2O_2 \rightarrow CaSO_4 \quad \text{(R4)}$$

Currently, there are challenges that need to overcome before the practical use of $CaSO_4$ oxygen carrier in a CLC system. One challenge is the low reaction rate of $CaSO_4$ with fuel, especially for

solid fuels, e.g. coal, which makes the CLC system needed to be operated under high temperature, this will give rise to sintering and deactivation of $CaSO_4$ oxygen carrier. Another challenge is the sulfur release (mainly in the form of SO_2), which is verified that the potential sulfur release results in a decline in the reactivity of $CaSO_4$ during the reduction/oxidation process. As illustrated in many investigations [19-23], the emission of sulfur involves with $CaSO_4$ and CaS is varied with the operating conditions. In this paper, SO_2 formation are mainly from the following side reactions during the reduction (R5-R8) and oxidation (R7-R9).

$$CaSO_4 + H_2 \rightarrow CaO + H_2O + SO_2 \quad \text{(R5)}$$

$$CaSO_4 + CO \rightarrow CaO + CO_2 + SO_2 \quad \text{(R6)}$$

$$CaSO_4 \rightarrow CaO + SO_2 + 1/2\,O_2 \quad \text{(R7)}$$

$$3CaSO_4 + CaS \rightarrow 4CaO + 4SO_2 \quad \text{(R8)}$$

$$CaS + 3/2\,O_2 \rightarrow CaO + SO_2 \quad \text{(R9)}$$

Although the sulfur-containing gases (such SO_2 and H_2S) can have a positive effect on fuel gasification to some extent [26], they will not only corrode the furnace and pipelines of CLC installation but also will present difficulties for CO_2 capture. As a consequence, measures used to improve the reactivity of $CaSO_4$ oxygen carrier and to minimize the release of sulfur species should be taken. Zheng et al. [22] investigated the effects of temperature and gasification intermediate on the reduction and sulfur release of $CaSO_4$ oxygen carrier with bituminous Shenhua coal. Liu et al. [27] employed different commercial powder and sols as binders to strengthen the mechanical strength of $CaSO_4$ and the results of thermogravimetric analysis showed that the addition SiO_2 could enhance the reduction rate of $CaSO_4$ with gaseous fuels. Zhang et al. [28] studied the reactivity of $CaSO_4$ and sulfur retention with CaO and $CaCO_3$ as desulfurizers, and desulfurization tests indicated that CaO provided higher desulfurization efficiency at higher temperature, higher pressure, and higher Ca/S ratio than $CaCO_3$. Song and Zhang [29, 30] investigated the influence of

Fe_2O_3 on the $CaSO_4$ oxygen carrier. Zhang [29] thought that the presence of Fe_2O_3 maybe could resist the sintering and agglomeration on the surface of $Fe_2O_3/CaSO_4$ particles, nevertheless Song [30] proposed that it was not the desulfurization capacity of iron oxide that lowered sulfur species emission but the suppression of the side reactions. In our research team, using Taguchi robust design method, the binder-supported $CaSO_4$ oxygen carriers prepared from the calcined $CaSO_4$, high sticky pseudo-boehmite (SB powder), acetic acid and water were investigated by intuitive analysis with the crushing strength and conversion as target functions and an optimal extrusion condition was obtained [31]. Besides, there are very few paper that report the reactivity enhancement and reduction of sulfur release of $CaSO_4$ oxygen carrier, especially in the coal-fueled CLC system.

Many research studies [32-34] have reported on the use of iron catalysts for the gasification of solid fuels, because iron is inexpensive but is one of the most promising catalysts. Asamil et al. [32] investigated gasification of brown coal and char with CO_2 using iron catalysts precipitated from an aqueous solution of $FeCl_3$. Comparison of the initial rates of uncatalyzed and catalyzed gasification revealed that iron addition could lower the reaction temperature by 120 ℃ and result in complete gasification within a short reaction time. Furthermore, previous studies [34] indicated that iron catalysts have higher carbon conversion and hydrogen production than alkali metal-based catalysts.

In the field of catalytic reduction of $CaSO_4$ to CaS, Fe_2O_3 was proved to be an efficient catalyst [35, 36]. In our previous study [35], $CaSO_4$ decorated with Fe_2O_3 was tested in a fixed-bed reactor and the result showed that Fe_2O_3 greatly improved the reactivity of $CaSO_4$, and CaS was the only reduction product. Li et al. [36] investigated the catalytic effect of various iron catalysts on reduction of $CaSO_4$ to CaS and discovered Fe_2O_3 could effectively promote the reduction reaction.

It is well-know that the mixed complex oxygen carriers may sometimes provide better properties than those of individual oxygen carrier [37-40]. Based on the obvious catalysis of Fe_2O_3, the

combination of active $CaSO_4$ with Fe_2O_3 as additive may create a synergy effect to improve the reactivity of $CaSO_4$ and to reduce the emission of sulfur-containing gases, similar like the synergy effect created by NiO/Al_2O_3 [39], CoO/NiO [38] and CuO/Fe_2O_3 [39, 40]. In this paper, experiments of gasification and CLC of char via steam medium in a batch fluidized-bed reactor were conducted for investigating the reactivity of $CaSO_4$ decorated with hematite. The effects of reaction temperature, iron-sulfur ratio (i.e. Fe_2O_3 loading content) and cycle numbers on the carbon conversion, the CO_2 yield, the SO_2 evolution rate as well as the synergy effect were investigated. Further, to explore the reaction mechanism, the fresh and reacted oxygen carriers were also characterized through X-ray diffraction (XRD), field emission scanning electron microscope equipped with energy dispersive spectrometer (FESEM-EDS), and pore structure analysis.

2. Experimental section

2.1. Material

The particles of $CaSO_4$ oxygen carrier used were produced from natural anhydrite ore, which was further crushed by pulverizer and sieved to size range of 180-250 μm. The natural anhydrite ore was composed largely of $CaSO_4$ and a small proportion of other impurity, as presented in Table 1. The apparent density and bulk density of the particles were 2950 and 1510 kg/m^3, respectively.

The mechanically mixed samples were prepared by mixing anhydrite particles with the particles of hematite. The high quality hematite from Australia was used as additives and the related components are given in Table 2. Due to the density of hematite particles was about twice than that of anhydrite, so hematite with particle diameter of 125-180 μm was chosen in order to avoid serious stratification phenomenon in a fluidized bed. Coal char selected as the solid fuel sample was prepared in the electric muffle furnace through calcining the bituminous Shenfu coal. It was also sieved for the particle diameter to be 400-500 μm. The proximate and ultimate analyses of the

Shenfu coal and coal char are summarized in Table 3. Coal ash contained 43.98% CaO, 15.68% SiO_2, 14.82% Fe_2O_3, 10.42% SO_3, 9.46% Al_2O_3 and some other minor phases by using X-ray fluorescence (XRF) analysis.

2.2. Experimental setup and procedure

Figure 1 shows the experimental setup used for testing the oxygen carriers. It consisted of a gas feeding, a fluidized reactor, a tube furnace, a cooler and a gas analysis system. A porous distributor plate was located in the middle stainless-steel tube (I.D. =40 mm, length =900 mm). The reactor was heated in an electric furnace, and the furnace temperature was controlled by a K-type thermocouple between the reactor tube and the heater, while the reaction temperature was monitored by another K-type thermocouple inside the oxygen carrier particles. The reactor had two connected pressure taps in order to measure the differential pressure in the bed and the monitor the fluidization state. In the tests, the coal particles were fed inside the fluidized bed with the help of a fuel chute. The upper part of the chute had a valve system that created a reservoir in which the coal particles were placed and later pressurized with N_2 to ensure quick coal particles feeding.

The flow rates of fluidizing gas and gasification agent were measured by mass flow controllers. The steam generator was composed of a TBP-5002 constant flow-type pump and a cast steel heater, and the steam mass flow was controlled precisely by adjusting the value of deionized water. The product gases from the reactor flowed through a cooler filled $CaCl_2$ desiccant which could condense the steam without the adsorption of acid or neutral gas, and then was sent to the gas analyzers. Three gas analyzers continuously measured the gas composition at each time. CO_2, CO and SO_2 gas concentrations as well as the gas flow at the outlet were measured by a GA-21 Plus flue gas analyzer, then the product gases were divided into two steams by a three-way valve. One gas steam was measured by a GASboard-3100 coal gas analyzer to detect the dry H_2 concentration; the other gas steam was measured by Geotech Biogas Check to measure the concentrations of CH_4 and O_2.

2.3. Experimental procedure

The experiments were performed in a laboratory fluidized bed reactor under atmospheric pressure using individual $CaSO_4$ or a mixture of $CaSO_4/Fe_2O_3$ as an oxygen carrier. In each run, 100 g of quartz sand with size range of 1 500-2 000 μm was added above the porous plate as preheating and distributing uniformly the reaction gas through the bed. Then a sample of 50 g $CaSO_4$ or $CaSO_4$ as well as a certain amount of hematite was placed on the quartz bed with the inside thermocouple located in the middle of the layer. During the preheating period, the reactor was purged with steam/N_2 gas flow. After the temperature reached the desired temperature and was kept stable, 1 g of coal char was quickly introduced to the bed under the pressurized effect of the instantaneous nitrogen supplement, then the reduction process began. When the reduction was finished, the gas flow of steam was turned off and the system was purged with N_2 flow until the product gases were cleared away, after which N_2 was replaced by the oxidizing gas for the subsequent oxidization period. A mixture of O_2 and N_2 (10% O_2/N_2) was introduced during oxidation until the outlet O_2 concentration reached the initial value, and then the gas was switched to N_2 for the next cyclic test. The lower O_2 concentration was used instead of air to avoid a large temperature increase because of the heat generated from the intense exothermic oxidation, since there was no installation to cool the reactor in the present setup.

When all tests were finished, the furnace was shut down. The sample was cooled in N_2 flow to ambient temperature and collected for further analysis. The N_2 concentration was not displayed in this study, and the specific experimental condition is shown in Table 4.

The compositions of the fresh and reduced samples were determined by XRD technique (X'pert Pro, Holland) using copper Kα radiation over a 2θ range of 15-85^o. The surface morphologies and element distributions of samples were measured by FESEM-EDS in a microscope system (Sirion 200, Holland). The pore structure properties of samples were measured by nitrogen

adsorption/desorption isotherms at 77 K with Micromeritics instrument ASAP 2020. The surface area and pore volume were calculated from the Brunauer-Emmett-Teller (BET) equations and Barrett-Joyner-Halenda (BJH) method, respectively.

2.4. Data evaluation

In order to quantitatively describe the relationship between gas compositions with time, the evolution rate of gaseous product $C_i(t)$ is the molar ratio of gaseous product species *i* per unit time to the total amount of carbon introduced to the FR and is calculated as follows:

$$C_i(t) = \frac{N_{i,\,out}(t)}{\Delta t \times N_{C,\,Fuel}} \quad (i = CO_2,\ CO,\ CH_4,\ H_2 \text{ and } SO_2) \tag{1}$$

The cumulative amount of gaseous product $X_i(t)$ is an integral result of the evolution rate, and is defined as:

$$X_i(t) = \frac{\sum_{t=0}^{n} N_{i,\,out}(t)}{N_{C,\,Fuel}} \quad (i = CO_2,\ CO,\ CH_4,\ H_2 \text{ and } SO_2) \tag{2}$$

The carbon conversion X_C is the ratio of carbon consumed to the carbon introduced to the FR, and is defined in the following equation:

$$X_C = \frac{\sum_{t=0}^{n}\left[N_{CO_2,\,out}(t) + N_{CO,\,out}(t) + N_{CH_4,\,out}(t)\right]}{N_{C,\,Fuel}} \tag{3}$$

The calculation of the carbon conversion X_C, an indirect measurement, is based on the main carbon-containing products (CO_2, CO and CH_4), so it ignores other carbon-containing species, such as tar, hydrocarbon and residual carbon in ash. For this reason, the carbon conversion X_C provided in the present study has to be understood and handled only as an apparent one. Meanwhile, on the basis the mass conservation, the carbon residue R_C could be calculated as follows:

$$R_C = 1 - X_C \tag{4}$$

However, the measurement of carbon residue is inevitably interfered with the reduced oxygen carrier. Thus, the value of R_C after individual char gasification is used instead. And the CO_2

selectivity formation $Y_{CO_2}(t)$ means the fraction of CO_2 in the carbon-containing species (CO_2, CO and CH_4) leaving the FR, this evaluation index gives a measure of the completion degree of combustion process in the FR and is defined as:

$$Y_{CO_2}(t) = \frac{\sum_{t=0}^{n} N_{CO_2,\,out}(t)}{\sum_{t=0}^{n}\left[N_{CO_2,\,out}(t) + N_{CO,\,out}(t) + N_{CH_4,\,out}(t)\right]} \tag{5}$$

The CO_2 yield η_{CO_2} is the ratio of the carbon converted to CO_2 to the carbon introduced to the FR. It is another way to evaluate the completion degree of the combustion process from the aspects of the products, and is calculated as:

$$\eta_{CO_2} = \frac{\sum_{t=0}^{n} N_{CO_2,\,out}(t)}{N_{C,\,Fuel}} = X_C \times Y_{CO_2} \tag{6}$$

For the convenience purpose, iron-sulfur ratio can be expressed as the addition amount of hematite divided by the amount of $CaSO_4$, which is written as Fe/S. Furthermore, in order to obtain reliable data, some repeated experiments were conducted.

3. Results and discussions

3.1. Performance of $CaSO_4$ oxygen carrier with coal char

The mass of coal char and $CaSO_4$ was 1.0 and 50 g, respectively. Under the 50 min present reaction time, the influence of temperature (900, 925, 950 and 975 ℃) on the product gas concentrations was investigated. The product gas evolution rate profiles as a function of time at typical reaction temperature of 900 and 975 ℃ are depicted in Figure 2. The peak times of product gases and variation trends were in line with the experiment results of char gasification, while the peak value of CO_2 evolution rate was more higher than that in char gasification experiment. This showed that char was gasified by steam, simultaneously the gasification products was oxidized by the $CaSO_4$ oxygen carrier particles to CO_2 and steam. The concentration of CO_2 was 40.56% at

900 ℃, and rose to 68.13% at 975 ℃, meanwhile the concentration of H_2 was lowered to 20.16% from 50.96%. On the one hand, it is an important factor which influenced the reactivity of char gasification and $CaSO_4$ reduction reaction. On the other hand, the existence of a large of H_2 and CO indicates that the reaction rate of $CaSO_4$ oxygen carrier with products of char gasification was lower. Therefore, further work is needed to enhance the reactivity with the purpose that $CaSO_4$ is utilized into large-scale CLC system.

3.2. Performance of $CaSO_4/Fe_2O_3$ oxygen carrier with coal char

3.2.1 Effect of reaction temperature

The effect of reaction temperature and reaction time on the reduction reaction of $CaSO_4$ oxygen carrier decorated with hematite was performed at the temperature of 850, 900, 925, 950 and 975 ℃. The mass of hematite was 6.5 g, and reaction duration time was 30 min. The other parameters of char mass, $CaSO_4$ mass and steam gas flow were kept constant (see Table 4).

Figure 3 displays evolution rates of product gases as a function of time during the reduction of $CaSO_4/Fe_2O_3$ with coal char at 850 and 950 ℃. Through a comparison of the Figures 3a and 3b, the peak of product gases appeared in advance and CO_2 evolution rate increased as the reaction temperature elevated. Other than that, as soon as the temperature was above 950 ℃, the results showed that char gasification was the control step of the reduction of $CaSO_4/Fe_2O_3$ with coal char, and the reduction of $CaSO_4$ had a sufficient rate to oxidized most of the gasification products to CO_2 and steam which was consistent with the conclusion of other researchers [22, 30]. Comparison to the Figure 2, the reactivity of $CaSO_4$ oxygen carrier modified by hematite was significantly enhanced. When the reaction temperature was below 900 ℃, the reduction rate of $CaSO_4$ with gasification products was lower than that of the char gasification. This led to a high concentration of H_2 and CO in the flue gas (Figure 4). As the reaction temperature increased, the chemical reaction rate constants

of both the char gasification reaction and the $CaSO_4$ reduction, especially the latter one, increased sharply. This difference in growth rates improved a partial pressure of the gasification mediums (CO_2 and H_2O) which might accelerate the char gasification process.

As shown in Figure 5, the H_2 evolution rate first increased to peak within the 5 min, and decreased markedly with the reaction temperature, which was also verified in the relevant literatures [22, 41]. Particularly at temperature of 925-975 ℃, the H_2 evolution rate was very low, and that H_2 was carried away by the flue gas flow, due to the shorter contact time between the char gasification products and $CaSO_4$. With the end of the char gasification reaction, the H_2 evolution rate reduced to zero. As the complicated reactions proceeded, the surface of $CaSO_4$ particles would be gradually covered by the generated CaS and small amounts of CaO, the gas products of char gasification firstly got through the CaS/CaO product layer, then reacted with $CaSO_4$ oxygen carrier. Thus, the reaction could be divided into two steps, earlier stage controlled by chemical resistance and the later stage controlled by chemical resistance and diffusion resistance, and this diffusion resistance increased.

The evolution rate of CO as a function of time during the reduction of $CaSO_4/Fe_2O_3$ with char is shown in Figure 6. At lower temperature (850-900 ℃), time to reach the peak was 4-5 min; Moreover, at higher temperature (925-975 ℃), time was only 3 min. Because of the weaker reactivity of $CaSO_4$ oxygen carrier at 850 ℃, part of unreacted CO was carried away by the flue gas flow. Within the temperature range of 900-975 ℃, the decay of $C_{CO}(t)$ increased with the increase of the temperature, and $C_{CO}(t)$ shrank to zero in the 15^{th} min. Compared to Figure 5, $C_{CO}(t)$ and $C_{H2}(t)$ were basically the same at the temperature of 900-975 ℃. Considering that the H_2 evolution rate was far greater than CO during the char gasification, so the reactivity of H_2 with $CaSO_4$ oxygen carrier was much higher than that of CO. This was in accordance to the previous thermodynamic analysis and experimental studies [22, 42].

The evolution rate of CO_2 as a function of time during the reduction of $CaSO_4/Fe_2O_3$ with char is

shown in Figure 7a. At lower temperature (850-900 ℃), time to reach the peak was 9-10 min; Moreover, at higher temperature (925-975 ℃), time was at least 1-2 min in advance, indicating the increase of temperature was beneficial to the formation of CO_2. The cumulative evolution rate of CO_2 (i.e. $X_{CO2}(t)$) as a function of time is presented in Figure 7b. Equilibrium would be reached when $dX_{CO2}(t)/dt$ reduced to zero. As shown in Figure 7b, the higher the temperature, the shorter the time reaching equilibrium were. The reason for this was that with regard to the chemical kinetics, a rise in the temperature led to an enhancement in the chemical reaction rate constant of char gasification and reduction.

The sulfur release from the coal/char was much lower in comparison with that from the side reactions [22]. In this study, SO_2 emission was dominant, which cumulative amount was nearly 20 times of H_2S. Meanwhile, H_2S was unstable which could be oxidized to SO_2 by the rest of $CaSO_4$. Thus, the H_2S evolution rate was not displayed. As indicated in Figure 8a, the curves of SO_2 evolution showed a single peak characteristic, and the peak time was delayed with the rising reaction temperature which was completely the opposite of the results of individual $CaSO_4$ oxygen carrier. Therefore it is reasonable to infer that the suppressed sulfur effect of hematite confirmed by song et al. [30], resulted in the delay of peak time of SO_2 release. From the Figure 8b, $X_{SO2}(t)$ increased with a rise of temperature, $X_{SO2}(t)$ at 975 ℃ was an order of magnitude higher than that at 850 ℃. Elevated temperature not only increased the reaction rate of principal reaction, but also increased that of the side reactions.

Figure 9 illustrates the carbon conversion, the carbon residue, the CO_2 selectivity formation and the CO_2 yield versus temperature. Among them, the carbon conversion, the CO_2 selectivity formation and the CO_2 yield increased with the increasing of temperature in the temperature range from 850 to 950 ℃. And the growth rates of the CO_2 selectivity formation and the CO_2 yield were significantly greater than that of the carbon conversion. As temperature was increased successively,

it was good for the char gasification, but bad for the reduction of $CaSO_4$. Because the sintering and agglomeration of oxygen carrier at 975 ℃ led to the reactivity decline of $CaSO_4$ oxygen carrier, which has been demonstrated by our and other research groups [21, 31]. Although the carbon conversion, the CO_2 selectivity formation and the CO_2 yield at 975 ℃ were still higher than that at 950 ℃, the growth rate was very small. And the main reasons of their growths come from two aspects: one is an excess of $CaSO_4$ oxygen carrier during the first reduction and the sintered $CaSO_4$ could be ignored, and the other is that more CO_2 was generated from the exothermic water-gas-shift reaction (R10).

3.2.2 Effect of iron-sulfur ratio

The iron-sulfur ratio was changed from 0.062 to 0.280 (i.e., the corresponding hematite mass was from 3.1 to 14.0 g) to investigate the effect on the combined process of char gasification and $CaSO_4$ reduction with gasification gases in the FR. The other operating conditions were kept constant: the reaction temperature (950 ℃), char mass (1.0 g), $CaSO_4$ oxygen carrier mass (50 g), steam flow rate (1.2 g/min), and set time (30 min). Figure 10 shows the variations of the product gas concentrations under four different Fe/S ratios. The CO_2 concentration was went up steady which was ascribed to the more hematite, while CO, H_2 and CH_4 concentrations were stable with a slight decline. Therefore, there was little influence on the product gas concentrations among the four Fe/S ratios, which was accordance with the conclusion by Li et al. [36].

The effect of Fe/S ratios on the evolution rate and cumulative evolution rate of SO_2 presented in Figure 11 shows the SO_2 evolution rate was gradually to reduce with an increase in Fe/S ratios, and the biggest decline range was 0.062-0.13. But within the range of 0.13-0.28, the drop was very limited. Hematite was firstly reduced by gasification gases (H_2, CO and CH_4) and then formed iron-based oxides catalyzed the reduction of $CaSO_4$ to CaS, which was good for the formation of

CO_2. Correspondingly, the side reaction of $CaSO_4$ to SO_2 may be suppressed. but when the mass of catalyst reached the maximum value of monolayer dispersion on the surface of $CaSO_4$, the further increase of CO_2 and decrease of SO_2 formation rates were limited to a certain extent. So there was no obvious influence on the suppressed sulfur release of $CaSO_4$ oxygen carrier when the Fe/S ratio reached 0.13. Considering the variation of product gas concentrations, especially for SO_2, the reasonable Fe/S ratio was 0.13.

3.2.3 Effect of cycles numbers

Five reduction/oxidation cyclic tests were carried out when Fe/S ratio was 0.13. The concentrations of flue gas as a function of cycle number are shown in Figure 12. As the number of cycles increased, the CO_2 concentration diminished gradually, accordingly, the CO concentration increased and its growth rate was obvious. It is evident that the reactivity of $CaSO_4$ after the reduction decreased gradually in the cyclic test, which was inconsistent with that of Ni-based oxygen carrier [41]. The possible reason of the decrease as follows: First, the release of sulfur species during the cyclic test led to the irreversible loss of oxygen atom in the $CaSO_4$ oxygen carrier and the decrease of the oxygen transport capacity; Second, due to the attachment of ash in char onto the outside surface of $CaSO_4$, the density oxidation film was formed which resulted in the increase of gas diffusion resistance of gasification products; Last, it is also entirely possible that the Ca-based oxygen carrier was sintered and broken because of the higher temperature and fluidizing velocity during the long cyclic tests.

After the 5 cyclic test, the total concentration of the combustible gas reached to about 20%. One possibility to address this incomplete gas conversion would be to separate the combustible gases from the CO_2 in connection with the liquefaction of CO_2. However, suitable processes and costs for achieving this were not well established. Another method of “oxygen polishing” was proposed by

Professor Lyngfelt [43], this meant that the combustible gases remaining in the gas from the FR were oxidized immediately after the cyclone by adding a stream of oxygen.

Figure 13 illustrates the cumulative evolution rates of SO_2 as a function of cycle number during the 5 cyclic test. The cumulative evolution rates of SO_2 in the reduction were significantly lower than that in the oxidization. Although the O_2 concentration in the oxidizing gas was artificially reduced and then the oxidization reaction rate was lowered, the exothermic nature of the oxidation reaction still led to the release of heat and a subsequent temperature rise in oxygen carrier particle which was favorable for the sintering of oxygen carrier and aggravation of the side reactions. On the other hand, the cumulative evolution rates of SO_2 in the reduction or oxidization decreased firstly and increased subsequently with the increase of cycle number. Combined with experimental conclusion in the 3.3.1 section, the decrease of the cumulative evolution rates of SO_2 was ascribed to the existence of hematite, and a detailed analysis is carried out in the following section with the characterization of oxygen carriers.

3.3. Characterization analysis

3.3.1 Phase characterization

The results of XRD analysis of fresh anhydrite and reacted $CaSO_4$ decorated with 6.5 g hematite of different reaction temperatures are shown in Figure 14. The presence of anhydrite ($CaSO_4$) as the main crystalline phase in the fresh natural anhydrite was clearly evidenced. Suppose all of char reacted with $CaSO_4$ oxygen carrier, then mass of $CaSO_4$ involved in the reaction was only occupying for about 11% of the whole $CaSO_4$ oxygen carrier. Thus, the peak intensity of CaS was significantly lower that that of $CaSO_4$. In addition, considering that CaS in sample could be easily oxidized by air at room temperature, the peak intensity of CaS was generally low in XRD patterns. Therefore, the ratio of the peak intensity of CaS to $CaSO_4$ could not be used to evaluate the extent of $CaSO_4$

reduction, but the ratio of that of CaO to $CaSO_4$ could be used to evaluate intensity of the side reactions, and the ratio with the increase of temperature was: 0.0192、0.0204、0.0347、0.0381, respectively. Hence, the side products (CaO and SO_2) increased gradually with the increase of temperature which was in line with SO_2 concentration analysis in the section 3.3.1. Within the temperature range of 900-950 ℃, only Fe_3O_4 was detected after the reduction which proved that all of hematite involved in the reduction reaction. However, the existence of $Ca_2Fe_2O_5$ at 975 ℃ suggested solid-solid reaction happened between hematite and CaO. Although $Ca_2Fe_2O_5$ as an inert support could improve the specific surface area and mechanical strength of oxygen carrier particles, oxygen transfer or catalysis of Fe_2O_3 was gradually weakened or even disappeared. In other words, 975 ℃ was not appropriate as reduction temperature of char-fueled CLC with $CaSO_4/Fe_2O_3$ oxygen carrier.

The results of XRD analysis of reduction products of $CaSO_4$ decorated with the different loading content of Fe_2O_3 and oxidation products of $CaSO_4$ decorated with 6.5 g hematite after the 5 cyclic test at 950 ℃ are shown in Figure 15. From the parts a to c of Figure 15, influence of Fe/S ratio on the reduction products was not obvious, and hematite was completely reduced to Fe_3O_4. After the 5 cyclic test, hematite still could exist in oxygen carrier as Fe_2O_3. As a consequence, hematite could continuously and effectively catalyze the reduction of $CaSO_4$ oxygen carrier at 950 ℃.

3.3.2 Surface morphology

According to the variations of surface microcosmic morphology of oxygen carrier before and after the reaction, such as grain size, crack and break of oxygen carrier particles, the changes in reactivity of oxygen carrier can be explained to some extent. In this section, the morphology features of oxygen carrier particles were analyzed using the FESEM before and after the reaction. Parts a and b of Figure 16 display the surface morphology of fresh anhydrite and fresh hematite, respectively. The

fresh anhydrite was compact and impervious, while the fresh hematite was more developed pore structure than anhydrite which was conductive to the diffusion of gasification product gases. After the first reduction at 950 ℃, as shown in part c of Figure 16, the surface of $CaSO_4$ oxygen carrier particles was rough and was composed of comparably sized grains which were not evenly distributed and moved closer together. And a small amount of grain aggregations was found on the surface of particles, which was in agreement with the previous study [21]. The crystal grains seemed to be formed as a consequence of the reduction reaction, the part of $CaSO_4$ was reduced to CaS and the molar volume decreased from 46.0 to 28.9 cm^3/mol. Therefore, it can be concluded that CaS would exist in pretty much the same form of evenly distributed grain, and unreacted $CaSO_4$ in state of aggregation [23]. The left-hand figure was an electron backscatter diffraction pattern (EBSP) in part d of Figure 16, and metal compounds (Fe_2O_3 or Fe_3O_4) and Ca-based compounds ($CaSO_4$, CaS or CaO) could be clearly distinguished through EBSP. Therefore the shiny particle was Fe_3O_4 in the middle of the left-hand figure. The appearance of the surface in part d of Figure 16 was basically similar to that shown in part c of Figure 16 with porosity and interstice. However, a different from the particle with hematite after the first reduction was that the number of aggregations reduced, grains were evenly distributed and small grains of a size around 2-3 μm became more. Figure 16e also indicates that there was not any sintering between oxygen carrier particles, and the oxygen carrier remained its beehive form after the 5 cyclic test. The majority of grains of a size around 1-2 μm were uniformly distributed on the surface of $CaSO_4$ oxygen carrier particles, which was advantageous to the reactive gases into the internal spaces of particles. The other interesting thing to note is that a small amount of particles became a little larger in a compact agglomerated state. It seems that the grains on the surface of the oxygen carrier may be sintered after more cyclic test, which would result in the decrease of surface area and reactivity of $CaSO_4$ oxygen carrier.

3.3.3 BET analysis

The BET surface area, pore structure and pore size distribution of fresh and used oxygen carrier particles are listed in Table 5. The BET surface area of fresh anhydrite was only 0.2573 m^2/g, which had great relations to the structure of anhydrite as presented in Figure 16a. The surface area and total pore volume of individual $CaSO_4$ oxygen carrier rapidly increased after the first reduction at 950 ℃, while the average pore diameter decreased. The increase of the BET surface area might be ascribed to the release of CO_2 and steam gases leaving the solid particles, which could be obviously observed in part c of Figure 16. Due to small amount of reacted $CaSO_4$ and inhomogeneous mixture of $CaSO_4$ and hematite, the surface area, average pore diameter and total pore volume of the $CaSO_4$ with 6.5 g hematite were near to that without hematite after the first reduction. However, the surface area of the $CaSO_4$ with hematite was up to 3.1466 m^2/g and the total pore volume reached 0.01728 cm^3/g after the 5 cyclic test, which was confirmed by part e of Figure 16, meanwhile the average pore diameter decreased sharply. Because of the larger contact area between hematite and Ca-based oxygen carrier under the fluidization and cyclic test, so the hematite not only played the role of an oxygen carrier, but it also had a great influence on the reactivity of $CaSO_4$ oxygen carrier. From the view of whole province, it is very interesting that the structural characteristics of $CaSO_4/Fe_2O_3$ oxygen carrier had the transition really into that of fresh hematite after the 5 cyclic test, and the related mechanism is still not known by now.

3.4. Catalytic mechanism analysis

3.4.1 Catalysis in gasification of char

Researcher have achieved consistency that alkali metals, alkaline-earth metals and transition metals (such as Fe and Ni) were the major source as active catalysts for steam gasification of coal/char [32-34]. During the steam gasification of coal/char, the gasification rate was proportional to the number of active sites on the chemical reaction boundary and active surface area. The addition

of catalysts was effective in increasing the active sites and active surface area, so the gasification rate was enhanced obviously [32]. The dispersion of iron catalyst can determine the activity during the char gasification, and the more highly dispersed iron was more active, but when the mass of catalyst reached the maximum value of monolayer dispersion on the surface of coal/char, the diffusion of gasification agent gas and escape of gasification product gases were suppressed, and the further increase of gasification rate was limited to a certain extent. Therefore, a suitable addition mass of catalyst did exist [34]. When Fe_2O_3 was added to char, H_2 and CO_2 concentrations increased in the gasification product gases, and CO decreased. The decrease of CO concentration could be ascribed to catalytic impact of Fe_2O_3 on the water gas shift reaction (R10). Although the effect of hematite on the char gasification was not investigated in this work, hematite could improve the gasification rate of char and the related schematic diagram is shown in Figure 17a.

3.4.2 Catalytic mechanism in the reduction

Under the influences of higher fluidization velocity as well as the collision between particles and the reactor wall, it is possible to infer that some grains broke off the hematite were attached to the $CaSO_4$ particles. Distributions of element Ca and Fe on the surface of the $CaSO_4/Fe_2O_3$ oxygen carrier after the 5 cyclic test are shown in Figure 18, which further verified the above-mentioned inference. As shown in Figure 17b, because hematite had the larger surface area and pore volume and the reactivity of hematite was proved to be better than that of $CaSO_4$ oxygen carrier [31], the gasification gas (such as H_2 and CO) was easily oxidized to form CO_2 and H_2O by hematite. And hematite was reduced to form Fe_3O_4, which was identified by XRD analysis. Furthermore, Fe-based oxide as a catalyst could reduce the activation energy of the reduction reaction between $CaSO_4$ oxygen carrier and reducing gases, and improve the reduction reaction rate. It is likely that the iron-catalyzed reduction proceeded through the oxygen-transfer mechanism involving the redox-cycle of iron oxides (R10-R12), as shown in Figure 17c. Ultimately, with the deepening of the

reduction and increasing of the cycle number, the probability of direct contact between $CaSO_4$ and Fe-based oxide reduced until that the generated CaS layer completely hindered the direct contact between Fe-based oxide and $CaSO_4$ oxygen carrier, which might result in the deactivation of iron catalyst as shown in Figure 17d. Then, the reducing gas need to diffuse the CaS layer and react with $CaSO_4$ oxygen carrier, and so the reaction rate of $CaSO_4$ reduction gradually lowered. Moreover, a previous study [34] indicated that Fe_2O_3 might react with side product CaO to form $Ca_2Fe_2O_5$. And the result of a CO_2 sorption test illustrated that the release of free Fe_2O_3 rarely occurred, as shown in the following equation (R13). To summarize, Fe-based oxide had the synergy effect on the $CaSO_4$ oxygen carrier with solid fuels, which could simultaneously catalyze both the steam gasification and the $CaSO_4$ reduction reaction, and suppress the side reactions. Further study needs to be conducted to clarify the mechanism of this synergy effect.

$$8Fe_3O_4+CaSO_4 \rightarrow 12Fe_2O_3+CaS \quad \text{(R10)}$$

$$3Fe_2O_3+CO \rightarrow 2Fe_3O_4+CO_2 \quad \text{(R11)}$$

$$3Fe_2O_3+H_2 \rightarrow 2Fe_3O_4+H_2O \quad \text{(R12)}$$

$$Ca_2Fe_2O_5+2CO_2 \rightarrow Fe_2O_3+2CaCO_3 \quad \text{(R13)}$$

4. Conclusions

In this study, experiments of gasification and CLC of char via steam medium in a laboratory scale fluidized-bed reactor were conducted for investigating the reactivity of $CaSO_4$ decorated with hematite. The effects of reaction temperature, iron-sulfur ratio and cycle numbers on the carbon conversion, the CO_2 yield, the SO_2 evolution rate as well as the surface morphology of oxygen carrier were discussed. And the main results are summarized as follows:

(1) A rise in the reaction temperature and hematite addition led to an enhancement of the carbon conversion and CO_2 yield. The peak values of SO_2 evolution increased with the rising reaction

temperature, but the peak time was delayed which was ascribed to the suppressed sulfur effect of hematite. The carbon conversion, the CO_2 selectivity formation and the CO_2 yield also increased with temperature, but iron-sulfur ratio had little influence on the product gas concentrations. Although the SO_2 evolution rate was to reduce gradually with an increase in Fe/S ratio, there was no obvious decrease for the SO_2 evolution rate when the Fe/S ratio exceeded 0.13.

(2) Five reduction/oxidation cyclic test was carried out, and results showed the reactivity of $CaSO_4$ decreased gradually in the cyclic test. The cumulative evolution rates of SO_2 in the reduction/oxidization decreased firstly and increased subsequently with the increase of cycle number. On the other hand, the cumulative evolution rates of SO_2 in the reduction were significantly lower than that in the oxidization.

(3) XRD analysis revealed hematite still can exist in oxygen carrier as Fe_2O_3 not $Ca_2Fe_2O_5$ after the 5 cyclic test; FESEM analysis demonstrated that there was not any sintering between oxygen carrier particles, and the oxygen carrier remained its beehive form after the 5 cyclic test. The majority of grains of a size around 1-2 μm were uniformly distributed on the surface of $CaSO_4$ oxygen carrier particles. BET analysis suggested the structural characteristics of $CaSO_4/Fe_2O_3$ oxygen carrier had the transition really into that of fresh hematite after the 5 cyclic test.

(4) According to the analyses above, Fe-based oxide had the synergy effect on the $CaSO_4$ oxygen carrier with solid fuels. The catalytic reduction mechanism of hematite was discussed, and the related chemical equations involving the oxygen-transfer mechanism of iron-catalyzed reduction were proposed.

Acknowledgements

This work was supported by the National Natural Science Foundation of China (Nos. 51406110, 51206102, 51276078), the Foundation for Outstanding Young Scientist in Shandong Province (No. BS2014NJ013) and the Youth Science Fund Project of Shandong Academy of Sciences (No. 2014N014). The authors were also grateful to the analytical and testing centers of Shandong Province and Huazhong University of Science and Technology for XRD, FESEM-EDS and BET measurements.

Nomenclatures

$C_i(t)$ evolution rate of gaseous product *i* (min^{-1})

n time elapsed since the reactions started in the FR (s)

$N_{i,\,out}(t)$ out molar amount of the products *i* within the interval Δt (mol)

$N_{C,\,Fuel}$ total molar amount of carbon introduced to the FR (mol)

R_C carbon residue

t time variable (s)

$X_i(t)$ cumulative amount of gaseous product *i* (min^{-1})

X_C carbon conversion

$Y_{CO_2}(t)$ CO_2 selectivity formation

Greek letters

η_{CO_2} CO_2 yield

References

1. N.N. Hlaing, S. Sreekantan, R. Othman, S.Y. Pung, H. Hinode, W. Kurniawan, A.A. Thant, A.R. Mohamed, C. Salime, Sol-gel hydrothermal synthesis of microstructured CaO-based adsorbents for CO_2 capture, *RSC Adv.* 2015, **5**, 6051-6060.
2. S.M. Hong, S.H. Kim, B.G. Jeong, S.M. Jo, K.B. Lee, Development of porous carbon nanofibers from electrospun polyvinylidene fluoride for CO_2 capture, *RSC Adv.* 2014, **103**, 58956-58963.
3. S.C. Tian, J.G. Jiang, K.M. Li, F. Yan, X.J. Chen, Performance of steel slag in carbonation-calcination looping for CO_2 capture from industrial flue gas, *RSC Adv.* 2014, **14**, 6858-6862.
4. M.C. Stern, T.A. Hatton, Bench-scale demonstration of CO_2 capture with electrochemically -mediated amine regeneration, *RSC Adv.* 2014, **4**, 5906-5914.
5. M. Sayyah, B.R. Ito, M. Rostam-Abadi, Y.Q. Lu, K.S. Suslick, CaO-based sorbents for CO_2 capture prepared by ultrasonic spray pyrolysis, *RSC Adv.* 2013, **3**, 19872-19875.
6. R. Sathre, E. Masanet, Prospective life-cycle modeling of a carbon capture and storage system using metal-organic frameworks for CO_2 capture, *RSC Adv.* 2013, **3**, 4964-4975.
7. N. Ding, W.R. Wang, Y. Zheng, C. Cong, P.F. Fu, C.G. Zheng, Development and testing of an interconnected fluidized-bed system for chemical looping combustion, *Chem. Eng. Technol.* 2012, **35**, 532-538.
8. Y. Cao, W.P. Pan, Investigation of chemical looping combustion by solid fuels. 1. Process analysis, *Energy Fuels* 2006, **20**, 1836-1844.
9. S.A. Scott, J.S. Dennis, A.N. Hayhurst, T. Brown, In situ gasification of a solid fuel and CO_2 separation using chemical looping, *AICHE J*. 2006, **52**, 3325-3328.
10. L.F. de Diego, M. Ortiz, J. Adánez, F. García-Labiano, A. Abad, P. Gayán, Synthesis gas generation by chemical-looping reforming in a batch fluidized bed reactor using Ni-based oxygen carriers, *Chem. Eng. J.* 2008, **144**, 289-298.
11. A. Lyngfelt, Chemical looping combustion of solid fuels – Status of development, *Appl. Energy* 2014, **113**, 1869-1873.
12. J. Adánez, A. Abad, F. García-Labiano, P. Gayán, L.F. de Diego, Progress in chemical looping combustion and reforming technologies, *Prog. Energy Combust. Sci*. 2012, **38**, 215-282.
13. P. Markström, C. Linderholm, A. Lyngfelt, Chemical looping combustion of solid fuels – Design and operation of a 100 kW unit with bituminous coal, *Int. J. Greenhouse Gas Control* 2013, **15**, 150-162.
14. T. Mendiara, L.F. de Diego, F. García-Labiano, P. Gayán, A. Abad, J. Adánez, On the use of a highly reactive ore in chemical looping combustion of different coals, *Fuel* 2014, **126**, 239-249.

15. R. Xiao, Q.L. Song, M. Song, Z.J. Lu, S. Zhang, L.H. Shen, Pressurized chemical looping combustion of coal with an iron ore-based oxygen carrier, *Combust. Flame* 2010, **157**, 1140-1153.

16. J.H. Bao, Z.S. Li, N.S. Cai, Experiments of char particle segregation effect on the gas conversion behavior in the fuel reactor for chemical looping combustion, *Appl. Energy* 2014, **113**, 1874-1882.

17. M.M. Hossain, H.I. de Lasa, Chemical-looping combustion (CLC) for inherent CO_2 separations – A review, *Chem. Eng. Sci.* 2008, **65**, 4433-4451.

18. H.E. Andrus, J.H. Chiu, P.R. Thibeault, A. Brautsch, *In: the 34th International Technical Conference on Clean Coal and Fuel Systems*, Clearwater, 2009.

19. H.J. Tian, Q.J. Guo, Investigation into the behavior of reductive decomposition of calcium sulfate by carbon monoxide in chemical looping combustion, *Ind. Eng. Chem. Res*. 2009, **48**, 5624-5632.

20. J. Wang, E.J. Anthony, Clean combustion of solid fuels, *Appl. Energy* 2008, **85**, 73-79.

21. Q.L. Song, R. Xiao, Z.Y. Deng, L.H. Shen, J. Xiao, M.Y. Zhang, Effect of temperature on reduction of $CaSO_4$ oxygen carrier in chemical-looping combustion of simulated coal gas in a fluidized bed reactor, *Ind. Eng. Chem. Res.* 2008, **47**, 8148-8159.

22. M. Zheng, L.H. Shen, J. Xiao, Reduction of $CaSO_4$ oxygen carrier with coal in chemical-looping combustion: Effects of temperature and gasification intermediate, *Int. J. Greenhouse Gas Control* 2010, **4**, 716-728.

23. Q.L. Song, R. Xiao, Z.Y. Deng, W.G. Zheng, L.H. Shen, J. Xiao, Multicycle study on chemical-looping combustion of simulated coal gas with a $CaSO_4$ oxygen carrier in a fluidized bed reactor, *Energy Fuels* 2008, **22**, 3661-3672.

24. M. Zheng, L.H. Shen, X.Q. Feng, J. Xiao, Kinetic model for parallel reactions of $CaSO_4$ with CO in chemical-looping combustion, *Ind. Eng. Chem. Res.* 2011, **50**, 5414-5427.

25. X. Rui, Q.L. Song, Characterization and kinetics of reduction of $CaSO_4$ with carbon monoxide for chemical-looping combustion, *Combust. Flame* 2011, **158**, 2524-2539.

26. R.K. Lyon, J.A. Cole, Unmixed combustion: An alternative to fire, *Combust. Flame* 2000, **121**, 249-261.

27. S.M. Liu, D.H. Lee, M. Liu, L.L. Li, R. Yan, Selection and application of binders for $CaSO_4$ oxygen carrier in chemical looping combustion, *Energy Fuels* 2010, **24**, 6675-6681.

28. S. Zhang, R. Xiao, Y.C. Yang, L.Y. Chen, CO_2 capture and desulfurization in chemical looping combustion of coal with a $CaSO_4$ oxygen carrier, *Chem. Eng. Technol.* 2013, **36**, 1469-1478.

29. S. Zhang, R. Xiao, J. Liu, S. Bhattacharya, Performance of $Fe_2O_3/CaSO_4$ composite oxygen carrier on inhibition of sulfur release in calcium-based chemical looping combustion, *Int. J. Greenhouse Gas Control* 2010, **4**, 716-728.

30. T. Song, M. Zheng, L.H. Shen, T. Zhang, X. Niu, J. Xiao, Mechanism investigation of enhancing reaction

performance with $CaSO_4/Fe_2O_3$ oxygen carrier in chemical looping combustion of coal, *Ind. Eng. Chem. Res.* 2013, **52**, 4059-4071.

31. N. Ding, Y. Zheng, C. Luo, Q.L. Wu, P.F. Fu, C.G. Zheng, Development and performance of binder-supported $CaSO_4$ oxygen carriers for chemical looping combustion. *Chem. Eng. J.* 2011, **171**, 1018-1026.
32. K. Asamil, R. Sears, E. Furirnsly, Gasification of brown coal and char with carbon dioxide in the presence of finely dispersed iron catalysts. *Fuel Process. Technol.* 1996, **12**, 139-151.
33. G. Domazetis, M. Raoarun, B.D. James, J. Liesegang, Molecular modeling and experimental studies on steam gasification of low-rank coals catalysed by iron species, *Appl. Catal. A-Gen.* 2008, **340**, 105-118.
34. B.S. Huang, H.Y. Chen, K.H. Chuang, R.X. Yang, M.Y. Wey, Hydrogen production by biomass gasification in a fluidized-bed reactor promoted by an Fe/CaO catalyst, *Int. J. Hydrogen Energy* 2012, **37**, 6511-6518.
35. N. Ding, Y. Zheng, C. Luo, Q.L. Wu, P.F. Fu, C.G. Zheng, Investigation into compound $CaSO_4$ oxygen carrier for chemical looping combustion, *J. Fuel Chem. Technol.* 2011, **39**, 161-168.
36. H.J. Li, Y.H. Zhuang, Catalytic reduction of calcium sulfate to calcium sulfide by carbon monoxide. *Ind. Eng. Chem. Res.* 1999, **38**, 3333-3337.
37. C. Dueso, A. Abad, F. García-Labiano, L.F. de Diego, P. Gayán, J. Adánez, A. Lyngfelt, Reactivity of a NiO/Al_2O_3 oxygen carrier prepared by impregnation for chemical looping combustion, *Fuel* 2010, **89**, 3399-3409.
38. H.G. Jin, T. okamoto, M. Ishida, Development of a novel chemical looping combustion: Synthesis of a looping material with a double metal oxide of CoO-NiO, *Energy Fuels* 1998, **12**, 1272-1277.
39. B.W. Wang, R. Yan, H.B. Zhao, Y. Zheng, Z.H. Liu, C.G. Zheng, Investigation of chemical looping combustion of coal with $CuFe_2O_4$ oxygen carrier, *Energy Fuels* 2011, **25**, 3344-3354.
40. B. Moghtaderi, H. Song, Reduction properties of physically mixed metallic oxide oxygen carriers in chemical looping combustion, *Energy Fuels* 2010, **24**, 5359-5368.
41. Z.P. Gao, L.H. Shen, J. Xiao, C.J. Qing, Q.L. Song, Use of coal as fuel for chemical looping combustion with Ni-based oxygen carrier, *Ind. Eng. Chem. Res.* 2008, **47**, 9279-9287.
42. L.H. Shen, M. Zheng, J. Xiao, R. Xiao, A mechanistic investigation of a calcium-based oxygen carrier for chemical looping combustion, *Combust. Flame* 2008, **154**, 489-506.
43. N. Berguerand, A. Lyngfelt, The use of petroleum coke as fuel in a $10kW_{th}$ chemical looping combustor, *Int. J. Greenhouse Gas Control* 2008, **2**, 169-179.

Figure Captions

Figure 1. Schematic diagram of the batch fluidized-bed reactor system.

Figure 2. Evolution rates of product gases as a function of time during the reduction of $CaSO_4$ with coal char in steam medium: (a) 900 ℃, (b) 975 ℃.

Figure 3. Evolution rates of product gases as a function of time during the reduction of $CaSO_4/Fe_2O_3$ with coal char in steam medium: (a) 850 ℃, (b) 950 ℃.

Figure 4. Product gas concentrations as a function of temperature during the reduction of $CaSO_4/Fe_2O_3$ with coal char in steam medium.

Figure 5. The evolution rates of H_2 as a function of time during the reduction of $CaSO_4/Fe_2O_3$with coal char in steam medium.

Figure 6. The evolution rate of CO as a function of time during the reduction of $CaSO_4/Fe_2O_3$with coal char in steam medium.

Figure 7. The evolution rate (a) and cumulative evolution rate (b) of CO_2 as a function of time during the reduction of $CaSO_4/Fe_2O_3$with coal char in steam medium.

Figure 8. The evolution rate (a) and cumulative evolution rate (b) of SO_2 as a function of time during the reduction of $CaSO_4/Fe_2O_3$ with coal char in steam medium.

Figure 9. Effect of reaction temperature on the carbon conversion, the carbon residue, the CO_2 selectivity formation and the CO_2 yield.

Figure 10. Effect of iron-sulfur ratio on the product gas concentrations.

Figure 11. The evolution rate (a) and cumulative evolution rate (b) of SO_2 as a function of Fe/S ratio during the reduction of $CaSO_4/Fe_2O_3$ with coal char in steam medium.

Figure 12. Effect of cycle number on the product gas concentrations.

Figure 13. The cumulative evolution rates of SO_2 as a function of cycle number.

Figure 14. XRD patterns of Ca-based oxygen carrier: (a) anhydrite, (b)-(c) $CaSO_4$ with 6.5 g

hematite during the different temperatures.

Figure 15. XRD patterns of Ca-based oxygen carrier at 950 ℃: (a) $CaSO_4$ with 3.1 g hematite, (b) $CaSO_4$ with 10.4 g hematite, (c) $CaSO_4$ with 14.0 g hematite, (d) $CaSO_4$ with 6.5 g hematite after the 5 cyclic test.

Figure 16. FESEM micrographs of the fresh and used oxygen carrier: (a) fresh natural anhydrite ore; (b) fresh hematite; (c) $CaSO_4$ after the first reduction at 950 ℃; (d) $CaSO_4/Fe_2O_3$ after the first reduction at 950 ℃; (e) $CaSO_4/Fe_2O_3$ after the 5 cyclic test at 950 ℃.

Figure 17. Schematic diagram of the mechanism of catalytic synergy effect: (a) catalytic gasification, (b) reduction of Fe_2O_3, (c) catalytic reduction of $CaSO_4$, and (d) deactivation of catalyst.

Figure 18. Distributions of element Ca and Fe on the surface of the $CaSO_4/Fe_2O_3$ oxygen carrier after the 5 cyclic test: (a) surface morphology of particles, (b) Ca, (c) Fe.

Figure 1.

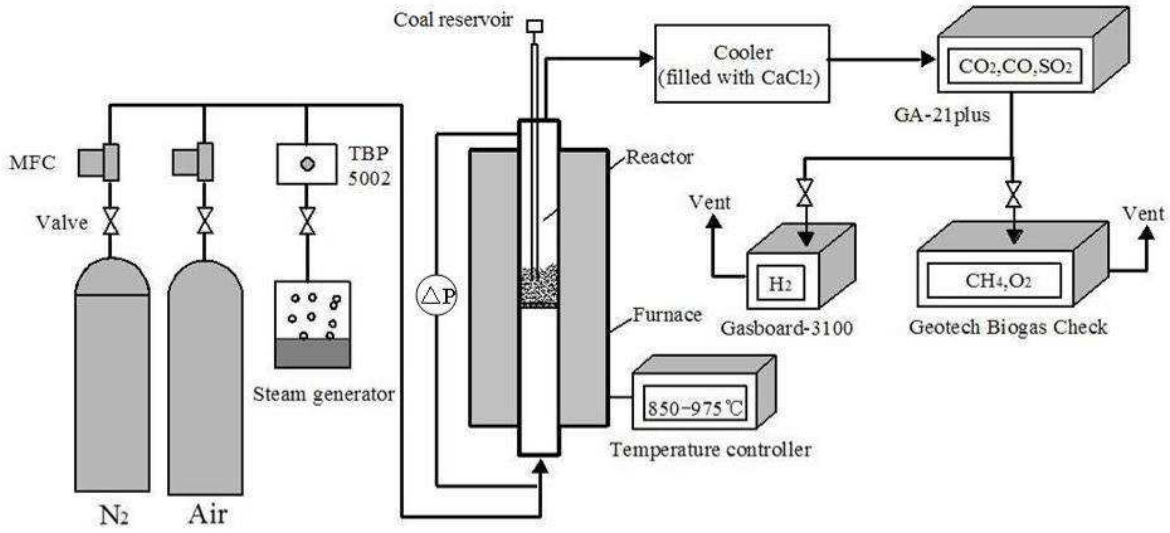

Figure 2.

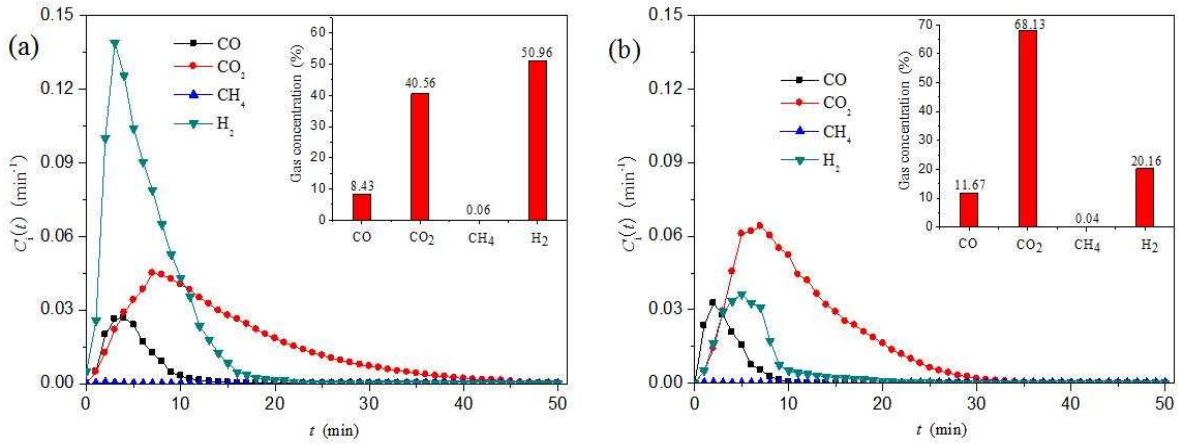

Figure 3.

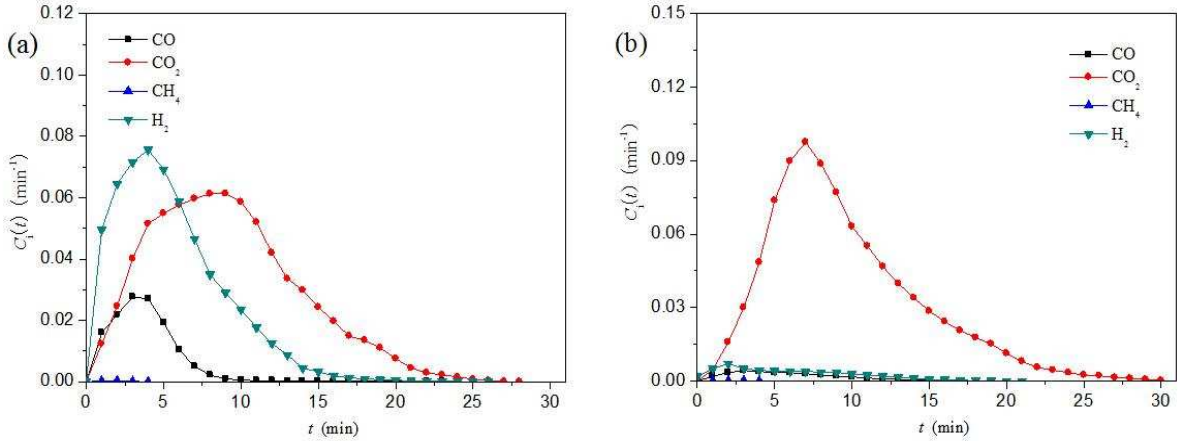

Figure 4.

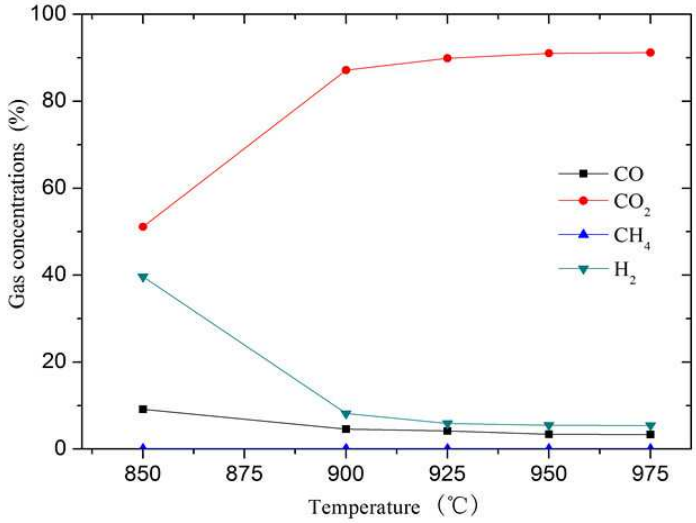

Figure 5.

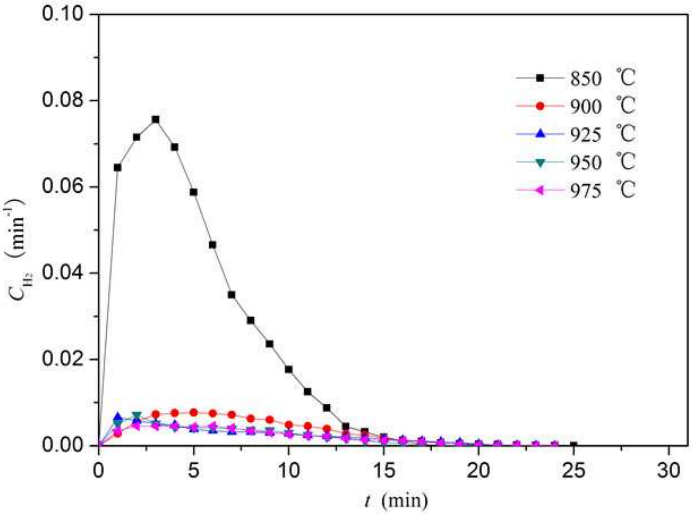

Figure 6.

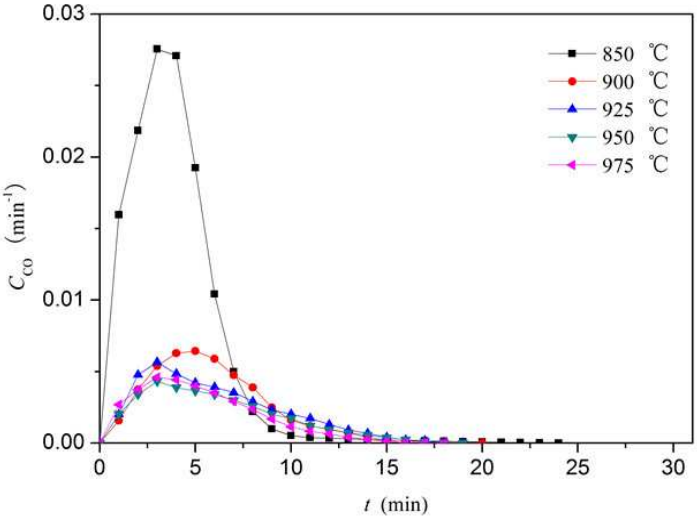

Figure 7.

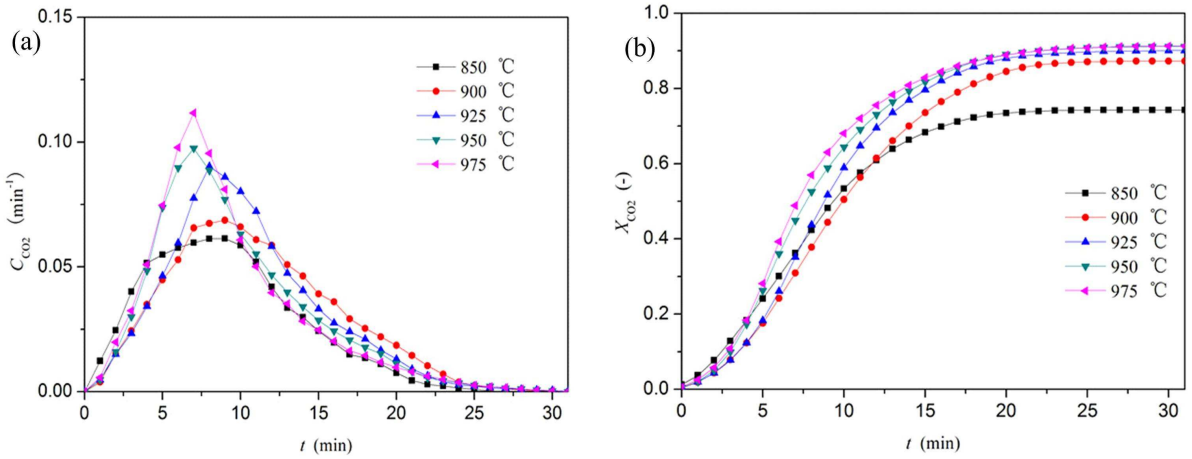

Figure 8.

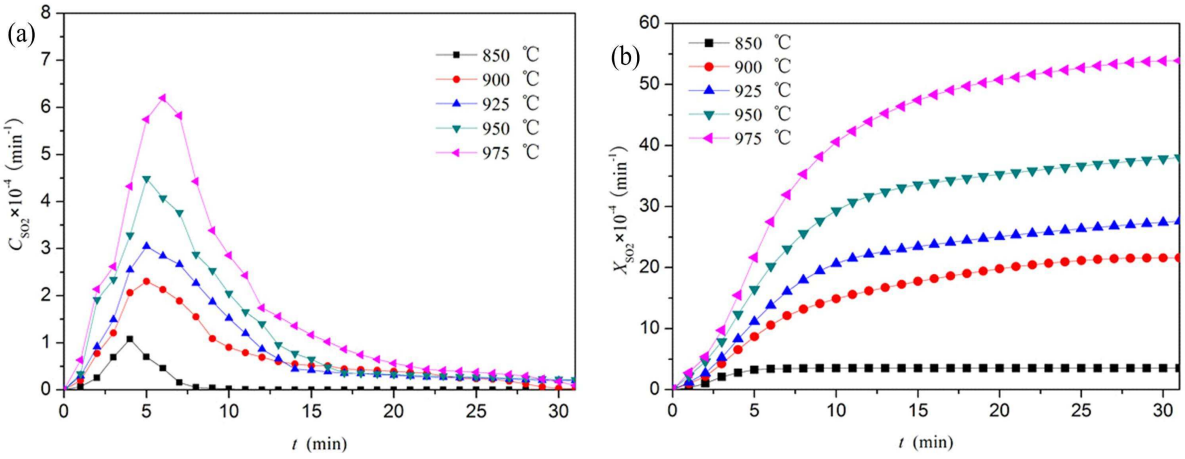

Figure 9.

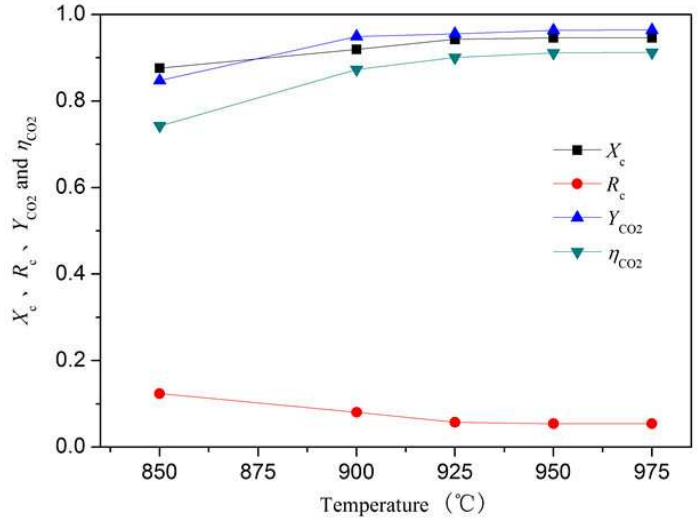

Figure 10.

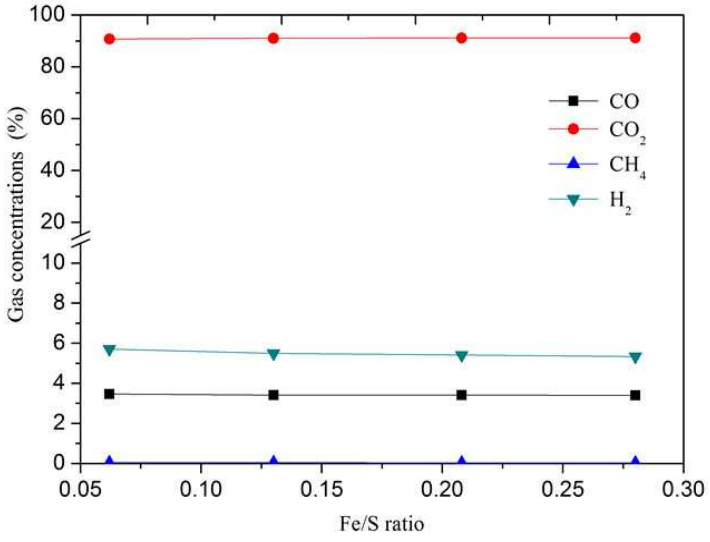

Figure 11.

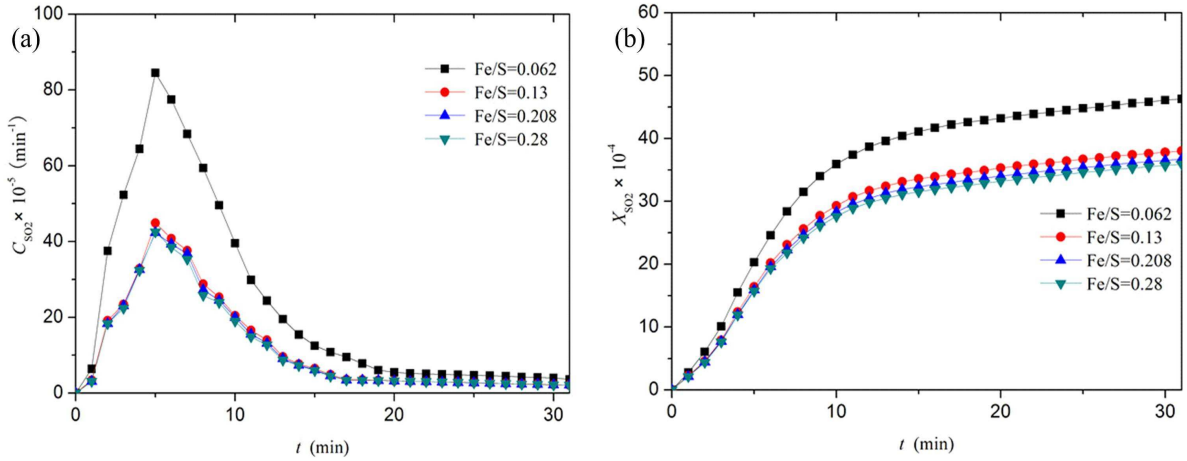

Figure 12.

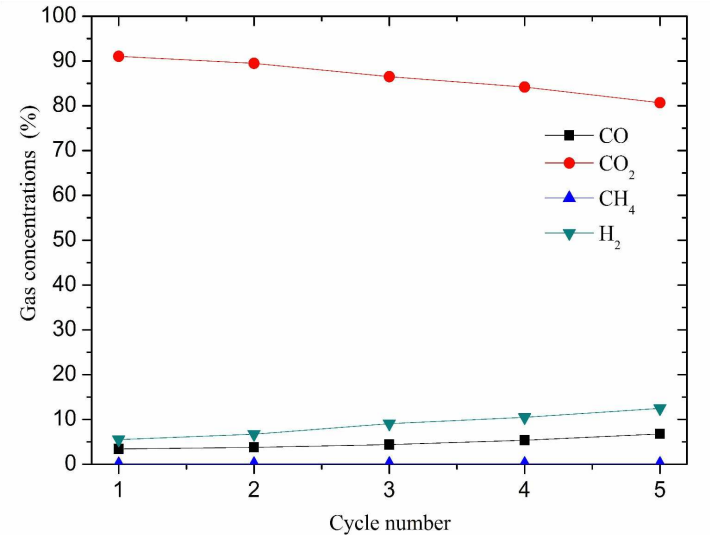

Figure 13.

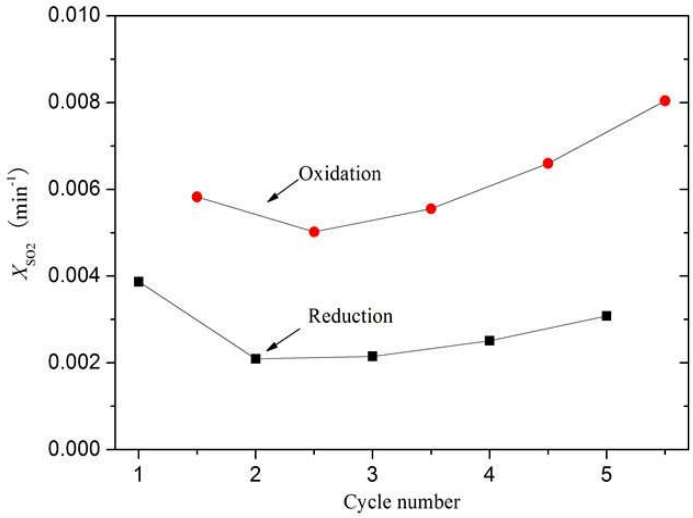

Figure 14.

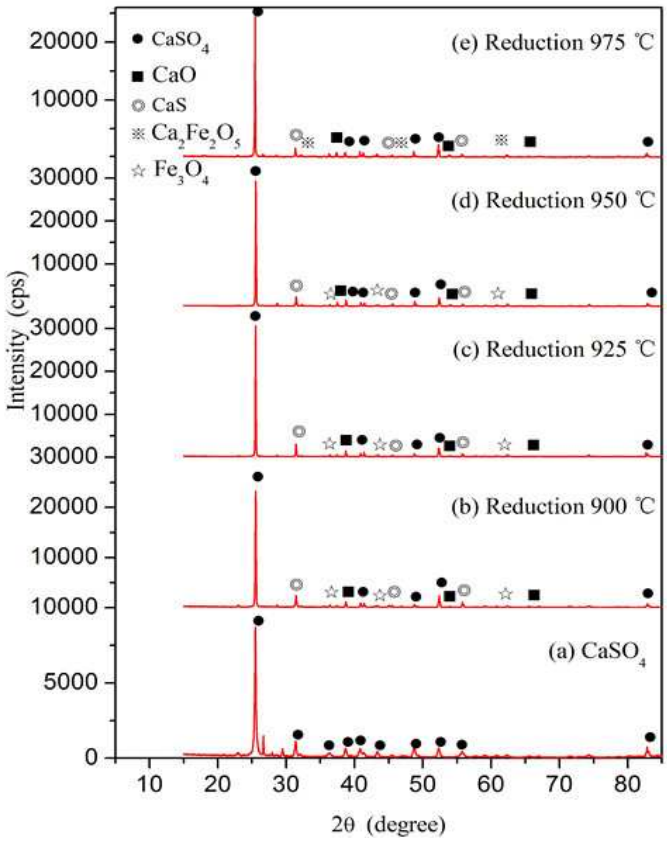

Figure 15.

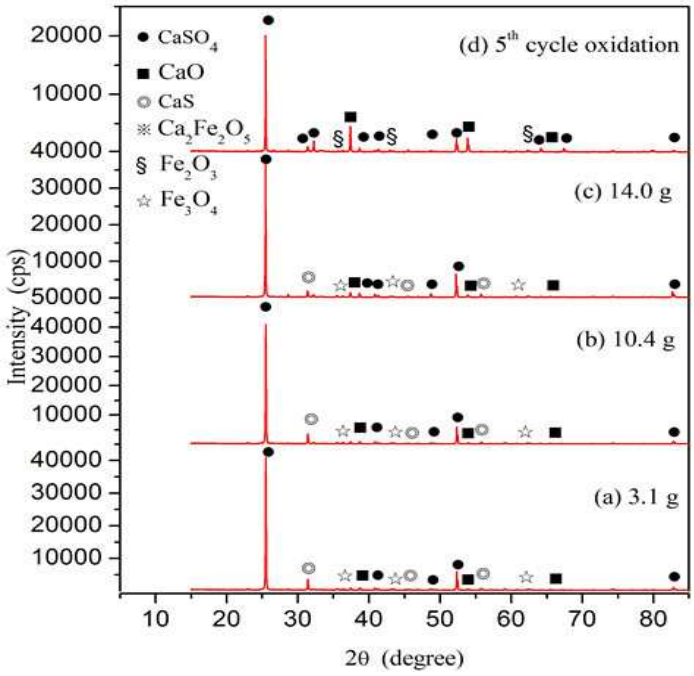

Figure 16.

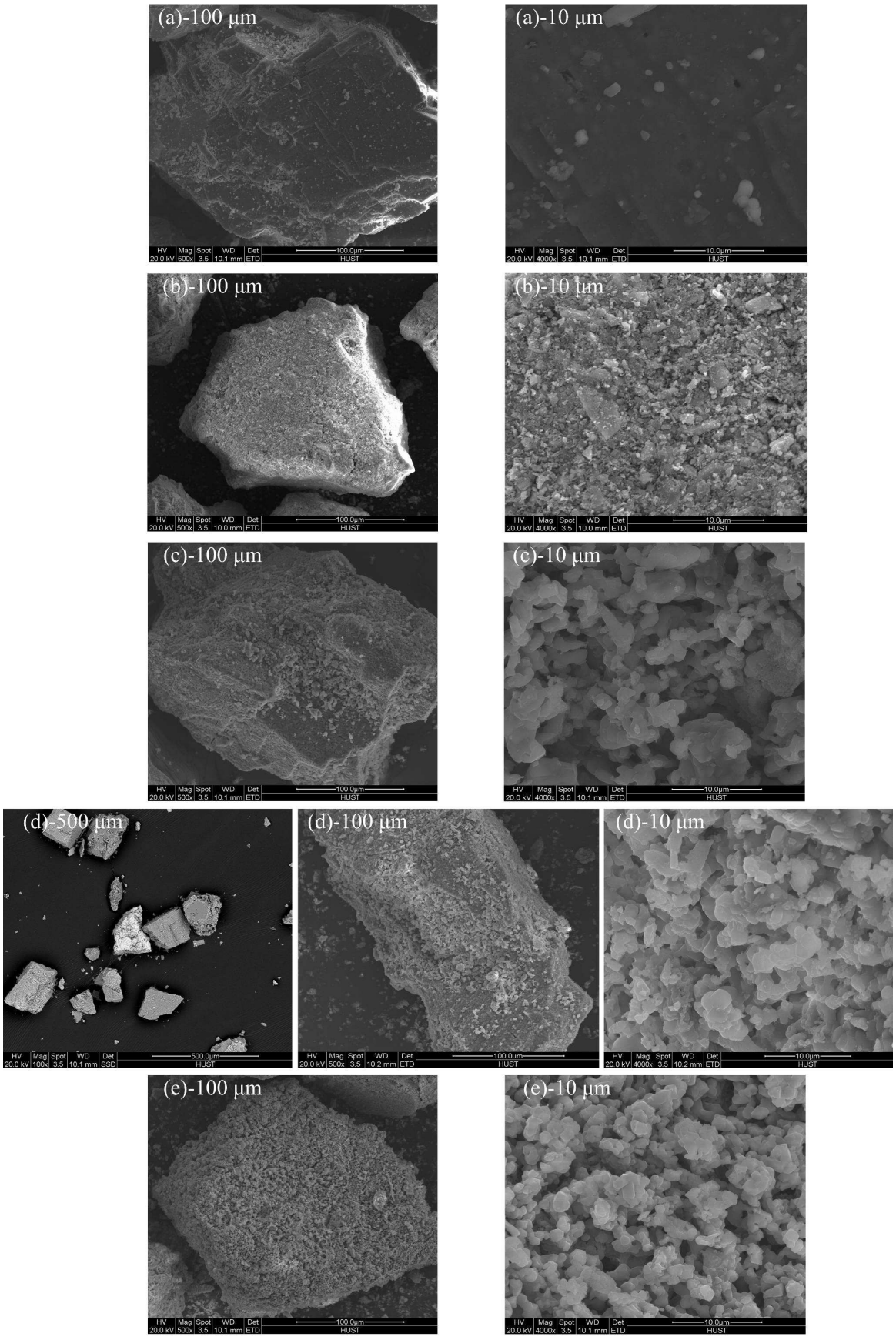

Figure 17.

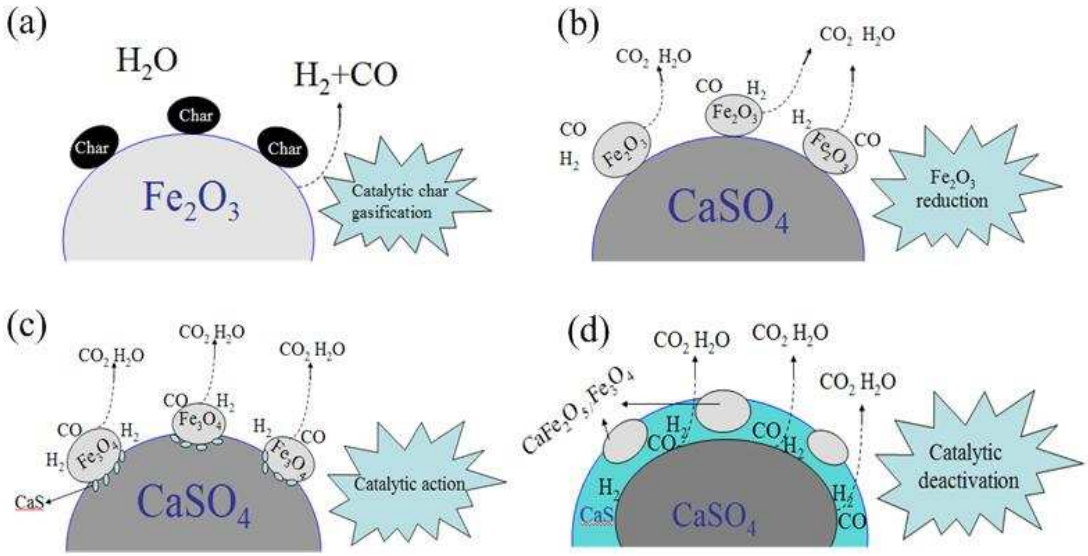

Figure 18.

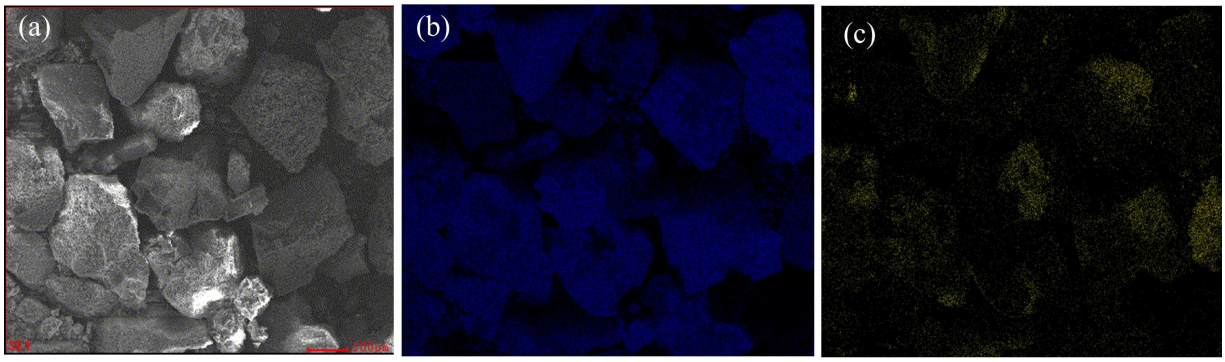

Table 1 Composition of natural anhydrite (wt %)

Chemical composition	Value
$CaSO_4$	95.02
CaO	1.25
SiO_2	0.65
MgO	0.46
Al_2O_3	0.25
TiO_2	0.05
Fe_2O_3	0.02
Crystallization water	2.30

Table 2 Composition of hematite (wt %)

Chemical composition	Value
Fe_2O_3	87.40
SiO_2	6.52
Al_2O_3	5.39
TiO_2	0.23
MgO	0.16
other	0.30

Table 3 Proximate and ultimate analysis of the Shenfu coal and coal char

Parameter	Coal	Char
Proximate analysis (wt %, as received basis)		
moisture	7.34	5.12
volatile	35.58	4.32
ash	4.65	10.32
fixed carbon	52.43	80.24
Ultimate analysis (wt %, dry basis)		
C	72.41	84.98
H	4.84	0.88
O	21.54	14.32
N	0.84	0.38
S	0.37	0.32

Table 4 Experimental condition

Oxygen carrier	$CaSO_4$ or $CaSO_4/Fe_2O_3$
Pressure (atm)	1
Reaction temperature (℃)	850, 900, 925, 950, 975
Particle size (μm)	$CaSO_4$: 180-250
	Fe_2O_3: 125-180
Particle mass (g)	$CaSO_4$: 50
	Fe_2O_3: 3.1, 6.5, 10.4, 14.0
Steam gas flow (g/min)	1.2
N_2 gas flow in reduction (ml/min)	300
Reduction time (min)	30, 50
Oxidation gas	O_2/N_2 = 10/90%
Oxidation gas flow (ml/min)	1150
Oxidation time (min)	50
Sweeping gas flow (ml/min)	1000

Table 5 Surface properties of fresh and used oxygen carrier particles

Species	BET surface area (m^2/g)	Total pore volume (cm^3/g)	Average pore diameter (nm)
Fresh anhydrite	0.2573	0.001475	45.1998
Fresh hematite	5.0380	0.025860	18.7569
$CaSO_4$-950 ℃-reduction	0.6996	0.004887	40.6276
$CaSO_4/Fe_2O_3$-950 ℃-reduction	0.7090	0.004085	44.3986
$CaSO_4/Fe_2O_3$-950 ℃-5 cycles	3.1466	0.017280	22.7888